Research in Pharmaceutical Sciences, June 2018; 13(3): 273-282
Received: December 2017
Accepted: February 2018

School of Pharmacy & Pharmaceutical Sciences
Isfahan University of Medical Sciences

Original Article

Preparation, process optimization and characterization of core-shell polyurethane/chitosan nanofibers as a potential platform for bioactive scaffolds

Laleh Maleknia[1,*], Mandana Dilamian[2], Mohammad Kazemi Pilehrood[3], Hojjat Sadeghi-Aliabadi[4], and Amir Houshang Hekmati[5]

[1]*Department of Biomedical Engineering, Islamic Azad University, South Tehran Branch, Tehran, I.R. Iran.*
[2]*Department of Textile Engineering, Faculty of Engineering, University of Guilan, Rasht, I.R. Iran.*
[3]*Nanotechnology Research Center, Islamic Azad University, South Tehran Branch, Tehran, I.R. Iran.*
[4]*Department of Medicinal Chemistry and Pharmaceutical Sciences Research Center, School of Pharmacy and Pharmaceutical Sciences, Isfahan University of Medical Sciences, Isfahan, I.R. Iran.*
[5]*Department of Textile Engineering, Islamic Azad University, South Tehran Branch, Tehran, I.R. Iran.*

Abstract

In this paper, polyurethane (PU), chitosan (Cs)/polyethylene oxide (PEO), and core-shell PU/Cs nanofibers were produced at the optimal processing conditions using electrospinning technique. Several methods including SEM, TEM, FTIR, XRD, DSC, TGA and image analysis were utilized to characterize these nanofibrous structures. SEM images exhibited that the core-shell PU/Cs nanofibers were spun without any structural imperfections at the optimized processing conditions. TEM image confirmed the PU/Cs core-shell nanofibers were formed apparently. It that seems the inclusion of Cs/PEO to the shell, did not induce the significant variations in the crystallinity in the core-shell nanofibers. DSC analysis showed that the inclusion of Cs/PEO led to the glass temperature of the composition increased significantly compared to those of neat PU nanofibers. The thermal degradation of core-shell PU/Cs was similar to PU nanofibers degradation due to the higher PU concentration compared to other components. It was hypothesized that the core-shell PU/Cs nanofibers can be used as a potential platform for the bioactive scaffolds in tissue engineering. Further biological tests should be conducted to evaluate this platform as a three dimensional scaffold with the capabilities of releasing the bioactive molecules in a sustained manner.

Keywords: Electrospinning core-shell; Nanofibers; Polyurethane; Chitosan

INTRODUCTION

The induction superior properties into a scaffold are effective strategy to tackle many challenges in tissue regenerations. These properties are consisted of high mechanical behaviors, surface functionality and the controlled release of bioactive macromolecules in an engineered scaffold (1). Coaxial electrospinning is a versatile method for the fabrication of two or more polymers in a form of a core-shell scaffold with three dimensional (3D) architecture. It is classified as a modified electrospinning, in way that a single capillary replaces with an inner capillary surrounded by outer tube.

In core-shell electrospun scaffold, the shell provides the bioactivity originated from biopolymer containing macromolecules while, a synthetic polymer as the core induces the mechanical and the structural integrity (1,2). Beside coaxial electrospinning, various techniques such as immersion coating (3,4), chemical conjugation (5,6) have been used to embed the bioactive molecules in nanofibers structure. However, they have been faced with some challenges leading to reduction of the versatility of electrospinning (1,7).

The electrospun scaffolds have two types of porosity including the porosity along the axis of fibers and the porosity between fibers.

*Corresponding author: L. Maleknia
Tel: +98-2166123234, Fax: +98-2166341439
Email: Melika02@azad.ac.ir

Access this article online

Website: http://rps.mui.ac.ir

DOI: 10.4103/1735-5362. 228957

Accordingly, the porosity between fibers plays a crucial role in the infiltration and the attachment of cells into a scaffold. In contrast, the porosity along fiber axis determines the performance of bioactive molecule release within the fibrous scaffolds.

These porosity properties have made the electrospun core-shell structure as an ideal candidate for the bioactive scaffolds. The controlled release, high loading efficiency and reduced initial burst release are paramount factors in a drug delivery system. In nanofibers- based drug delivery systems, the structures obtained from the direct electrospinning have the initial burst release leading to reduced efficiency of drugs. In contrast, core-shell structure prolongs the release time and preserves the structural integrity while maintains the bioactivity of molecules embedded into electrospun fibers (8-10). The structural properties of core-shell nanofibers such as fiber diameter, pore size, porosity and scaffold percolative efficiency play a crucial role to promote biological applications. As an example, for successful attachment and permeation of bladder smooth muscle cells, the optimal pore sizes in a scaffold should be designed almost 100-300 μm (11) and for skin regeneration are 20-125 μm (12) while this value for chondrocyte ingrowth is assumed to be almost near 70 and 120 μm (13). On the other hand, it is assumed that the increased fiber uniformity promotes morphological properties and leads to enhancing their mechanical features in a core-shell scaffold (14).

Beyond fabrication method and structural characteristics, the materials selection is another key element to exploit cell-scaffold interactions, leading to the highest mimicking *in vivo* environment. Chitosan (Cs) as a nontoxic, biocompatible and biodegradable polymer, in fibrous form was used as a scaffold (15-20), a wound dressing (21,22) or a bioactive molecules delivery system (23-26). Neat Cs is difficult to electrospin without blending with cospinning polymers. The composition of chitosan with cospinning polymers such as polyethylene oxide (PEO) can lead to higher chain entanglement, which is a main factor for obtaining the defect free nanofibers (7,27). In addition, blending of Cs with other polymers may induce the higher biochemical similarities of the scaffold compares to extracellular matrix components (EMC), leading to ameliorate the properties required in tissue repairs (7). In addition, polyurethane (PU) nanofibers were reported both as a scaffold (28,29) and drug release medium (30,31) in previous literatures.

The aim of this work is to produce core-shell PU/Cs nanofibers for the first time by one-step coaxial electrospinning, while PU was used as the core material and Cs/PEO were utilized as the shell component. The effects of different parameters such as solvent and polymer concentrations were investigated. Several methods including scanning electron microscopy (SEM), transmission electron microcopy (TEM), image analysis, Fourier transform infrared spectroscopy (FTIR), X-ray diffraction (XRD), differential scanning calorimetry (DSC), and thermogravimetric analysis (TGA) were exploited for characterization of these scaffolds. This study was tried to highlight only the design of potential platform for the bioactive scaffolds based on process optimization, as well as the quantification of their properties using standard techniques. Further biological tests should be conducted to evaluate this platform as a tissue scaffold with capabilities to release of drugs and bioactive molecules in sustained manner.

MATERIALS AND METHODS

Materials

Low molecular weight chitosan (molecular weight (MW), 120 kDa; degree of deacetylation (DD), 75-85%) was obtained from Fluka, Switzerland. Polyethylene oxide (MW, 900 kDa) was purchased from Sigma Aldrich, USA. Polyurethane was obtained from Esthane Thermoplastics. Dimethylformamide (DMF) and tetrahydrofuran (THF) were purchased from Merck, USA.

Electrospinning of PU, Cs/PEO, and core-shell PU/Cs nanofibers

PU solution (7.5 wt%) prepared by dissolving PU in THF /DMF blend solvent at different volume ratios including 100:0, 90:10, 80:20, 70:30, 60:40, 50:50, 40:60, 30:70,

20:80, 10:90, 0:100. The prepared solutions were electrospun by variation of applied voltage (15, 18, 20 kV) and different needle-collector distance (10, 12, 14 cm). The electrospinning was performed by Electroris (Fananvaran Nano-Meghyas). In the next step, PU solutions at 4, 6, 7.5, 8, 9, 10 wt% were prepared by dissolving PU in THF/DMF (60:40%) blend solvent and electrospinning was performed at constant voltage 15 kV, needle-collector distance 12 cm, and corresponding flow rate 0.2 mL/h. It was observed the optimal PU concentration for electrospinning mechanism was 7.5 wt% in 60:40 blend THF/DMF. Meanwhile, a chitosan/PEO solution in 2.5 wt% with a mass ratio of 75:25 was prepared by dispersion of chitosan or PEO in 90% acetic acid as described in a previous work (26) and was electrospun at 15 kV and needle-cylindrical drum of 12 cm. PEO was used as a cospinning component in the Cs solution to avoid any structural imperfections in the electrospinning of chitosan. The PU solution (7.5 wt%) and Cs-PEO solution (2.5 wt%) were added simultaneously to plastic syringe with 22/16 core-shell needle. The syringe was fixed in syringe pump and the needle was connected to cathode electrode. Core-shell PU/Cs nanofibers were electrospun at the optimized processing parameters (voltage 15 kV, needle-cylindrical drum of 12 cm, and flow rate 0.2 mL/h (7)). In this work, core-shell nanofibers constituted from blending of Cs and PEO as the shell component, in a mass ratio of 75:25, while PU was as the core counterpart. Because PEO is cospinning agent in the electrospinning process the resultant structure was considered as PU/Cs core-shell nanofibers.

Scanning and transmission electron microscopies

PU nanofibers and core-shell PU/Cs nanofiber scaffold were gold coated and their surface morphologies were observed by using a scanning electron microscope (SEM XL30, Philips). Core-shell PU/Cs structure was characterized by transmission electron microscopy (TEM, ZEISS, USA).

Image analysis

The structural characteristics measurements were carried out based on an image analysis and local criterion that was presented in details in our pervious papers (7,32). Overall porosity was measured by projection of fibrous network (solid area) in a two dimensional plane, while the interconnectivity was evaluated by the rate of blocking of the open channels in the depth of scaffold profile. The pore size was estimated by the measurement of the maximum Feret diameter. Mean fiber diameter was estimated by 20 measurements for each sample scaffold. Scaffold percolative efficiency (SPE) was determined by dividing overall porosity on the reciprocal of interconnectivity index obtained from regression analysis of layered porosity (the slope of the best-fit curve). The proposed simulation and measurements were implemented by ImageJ version 1.51q (National Institutes of Health (NIH)).

Fourier transform infrared spectroscopy and X-ray diffraction

FTIR investigations of PU nanofibers, Cs/PEO nanofibers, and core-shell PU/Cs nanofibers were carried out by using FTIR spectrophotometer (Bomem- MB 100 Series; Hartmann and Broun, rsqb). The samples were placed into FTIR spectrophotometer and IR spectra measurements were recorded in the wave number range of 500-4000 cm^{-1}. PU nanofibers, Cs/PEO naofibers, and core-shell PU/Cs nanofibers crystal structures were determined by using X-Ray diffractometer (D/max 2500 XRD spectrometer; Rigaku)

Differential scanning calorimetry and thermogravimetric analysis

Cs/PEO nanofibers, PU nanofibers and core-shell PU/Cs nanofibers were investigated by differential scanning calorimetry (DSC) using a SCINCO STA S-1500. Thermogravimetric analyses were conducted using dried samples for these three nanofibers on a thermoanalyzer TGA simultaneous SDT 2960 TA instruments.

RESULTS

The surface morphologies of the PU nanofibers at various ratios of THF/DMF blend solvent are shown in Fig.1a-f. PU solutions were electrospun successfully to the beadless fibers, except the solution had a THF/DMF composition of 0:100.

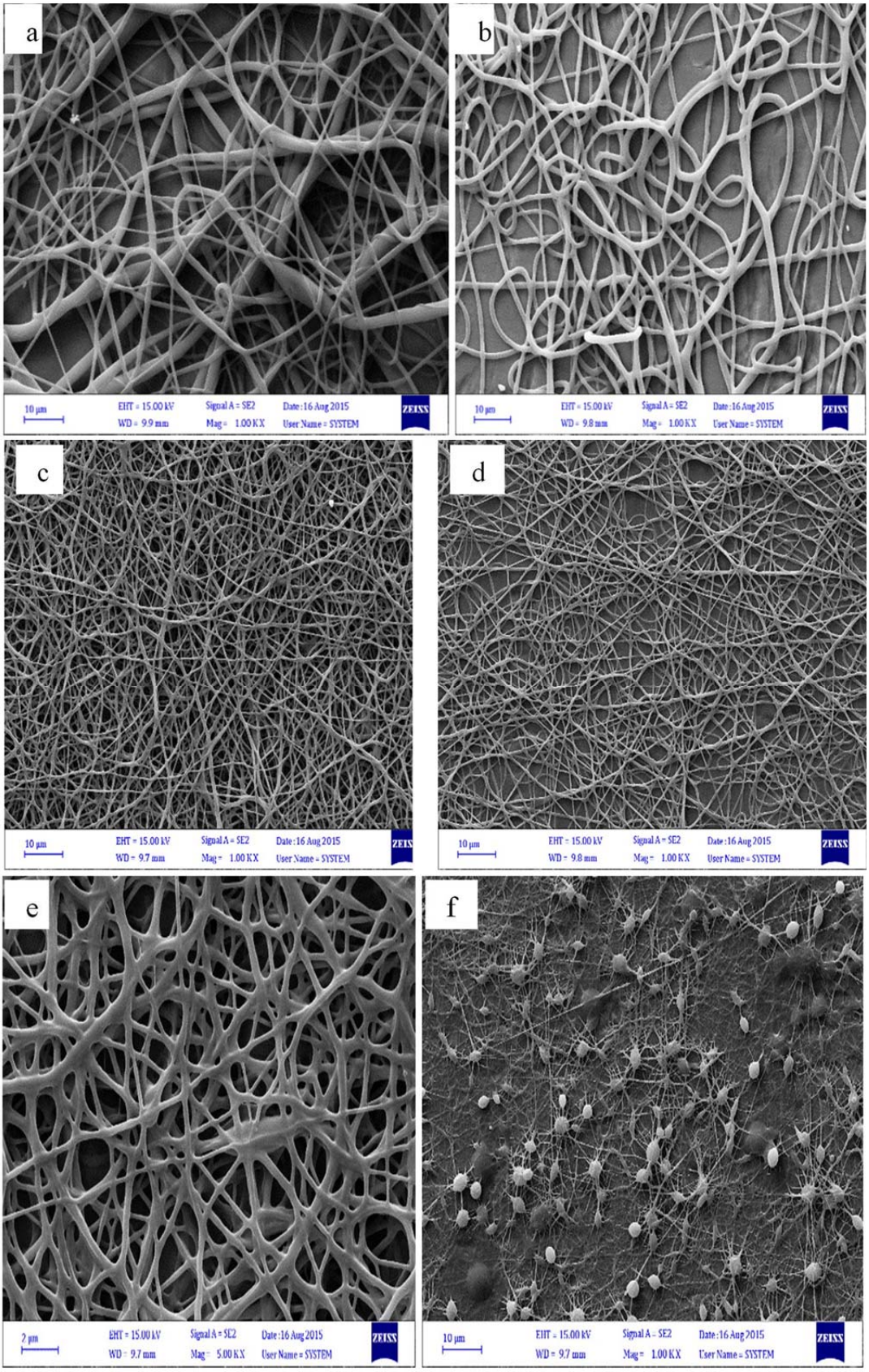

Fig. 1. SEM images of PU (7.5%). THF:DMF volume ratio of (a) 100:0, (b) 70:30, (c) 60:40, (d) 50:50, (e) 30:70, (f) 0:100, (voltage, 15 kV; needle-collector distance, 12 cm; and flow rate, 0.2 mL/h). SEM, scanning electron microscopy; PU, polyurethane; THF, tetrahydrofuran; DMF, dimethylfomamide.

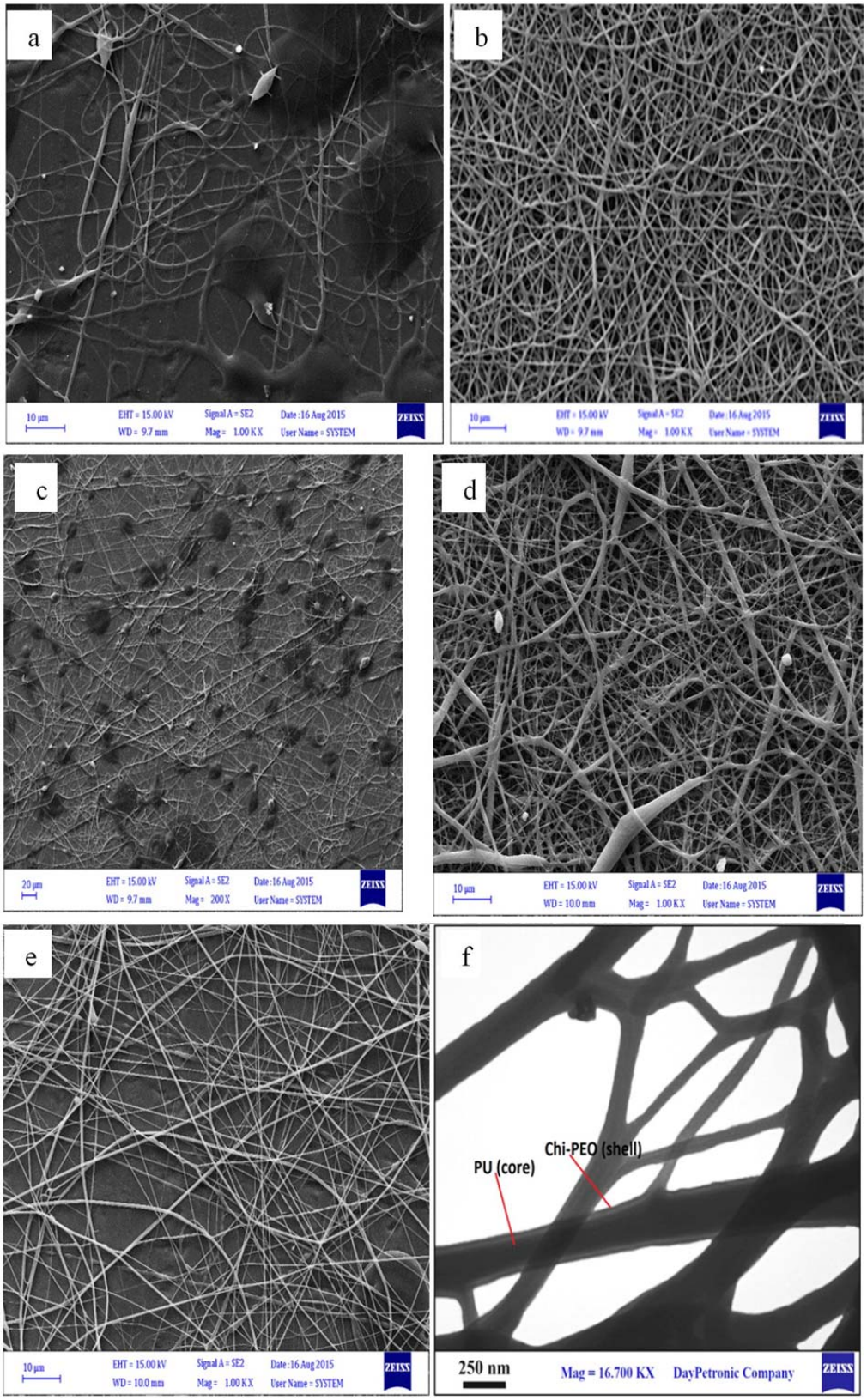

Fig. 2. SEM images of PU nanofibers at different concentrations. (a) 4 wt%, (b) 7.5 wt%, and (c) 8 wt%. SEM images of core-shell PU/Cs nanofibers (7.5 and 2.5 wt % respectively); THF:DMF ratio of (d) 60:40 and (e) 50:50 at constant voltage 15 kV, needle-collector distance 12 cm and flow rate 0.2 mL/h. (f) TEM image of core-shell PU/Cs nanofibers. SEM, scanning electron microscopy; PU, polyurethane; THF, tetrahydrofuran; DMF, dimethylfomamide; TEM, transmission electron microcopy.

SEM images of PU nanofibers at different concentrations are shown in Fig. 2a-c. In addition, Fig. 2d-e exhibited core-shell PU/Cs nanofibers in different THF/DMF compositions.

TEM image of core-shell structure was shown in Fig. 2f. FT-IR spectra for PU, Cs-PEO and core-shell PU/Cs nanofibers are shown in Fig. 3. The spectrum of Cs-PEO nanofibers reflected C-H_2 bending by showing peak at 868 cm^{-1} whereas peaks at 1070-1101 cm^{-1} range and 1166 cm^{-1} traced back to stretching of carbonyl (C-O-C) bands. In addition, secondary amine (NH2) stretching band and amine I stretching band at C=O-NH are demonstrated at 1543 cm^{-1} and 1634 cm^{-1}, respectively. Peak at 2853 cm^{-1} is the sign of the C-H band as well as peak at 2924 cm^{-1} showed the symmetric vibrations of CH_2 in CH_2-OH. Also a strong broad band was observed at 3432 cm^{-1} attributed to -OH groups and vibrations of NH_2 bands. FT-IR spectra of PU nanofibers showed peak at 1100-1248 cm^{-1} range reflected the asymmetric stretching of C-O-C while the peaks at 1607 cm^{-1}, 1349 cm^{-1} and 1462 cm^{-1} were related to the -CH_2 and -CH_3 vibrations. In addition, band at 1731 cm^{-1} attributed to the PU carbonyl (C=O) vibration. Peak at 2882 cm^{-1} exhibited CH_3 symmetric groups while the broadband at 3431 cm^{-1} was attributed to N-H bands stretching. The core-shell PU/Cs nanofibers obtained from FTIR spectra exhibited the peaks at 1260 cm^{-1}, 1380 cm^{-1}, 1533 cm^{-1}, and 1630 cm^{-1} attributed to C-C band in PU, amine III band in Cs, C-C in PU and amine I band in Cs, respectively. Furthermore, a strong broadband was observed at 3435 cm^{-1} due to the -OH groups and N-H stretching vibration. The bands below 800 cm^{-1} traced back to the C-H and N-H out-of-plane degrees of freedom.

XRD patterns for PU nanofibers, Cs-PEO nanofibers, and core-shell PU/Cs nanofibers were shown in Fig. 4. The XRD pattern reflected the crystallinity of nanofibous structure. Diffraction peaks were observed at 20.64° and 22.07° for the Cs-PEO nanofibers. These peaks attributed to Cs I and II crystalline phase. Diffraction peaks at 19° and 20.05° for the PU nanofibers were attributed to their crystalline phase.

The resultant XRD pattern for core-shell PU/Cs nanofibers exhibited peak at 19.56° at the same range for neat PU nanofibers (peak 19°).

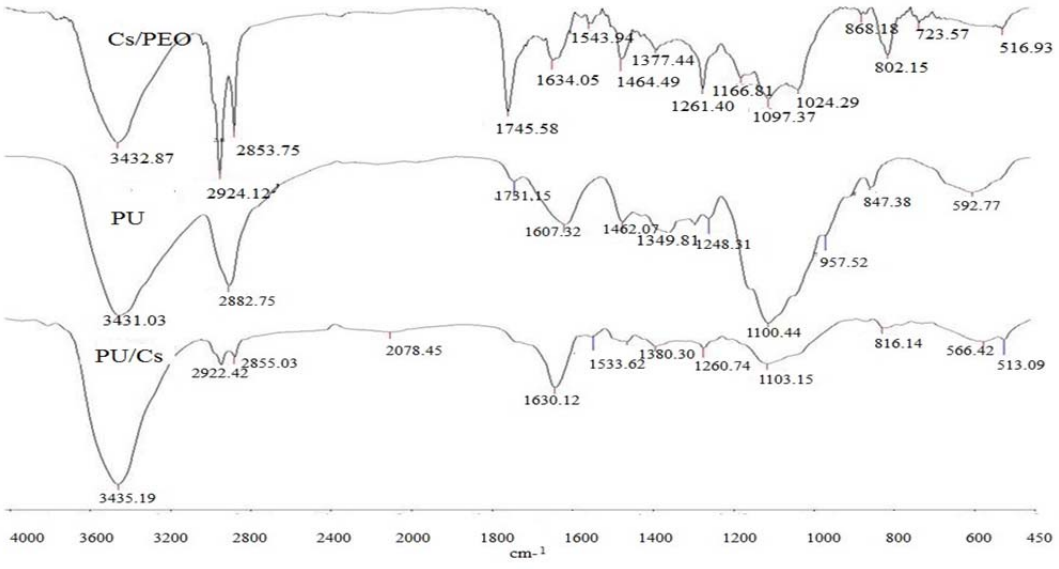

Fig. 3. FTIR spectra. PU, Cs/PEO and core-shell PU/Cs nanofibers. FTIR, Fourier transform infrared spectroscopy; PU, polyurethane; Cs, chitosan; PEO, polyethylene oxide.

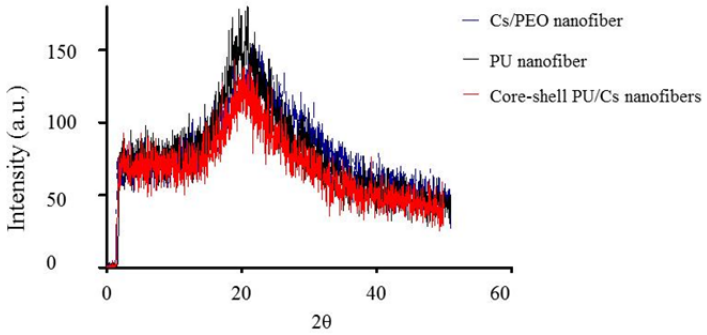

Fig. 4. X-ray diffraction patterns of Cs/PEO (blue curve), PU (black curve), core-shell PU/Cs nanofibers (red curve). Cs, chitosan; PEO, polyethylene oxide; PU, polyurethane.

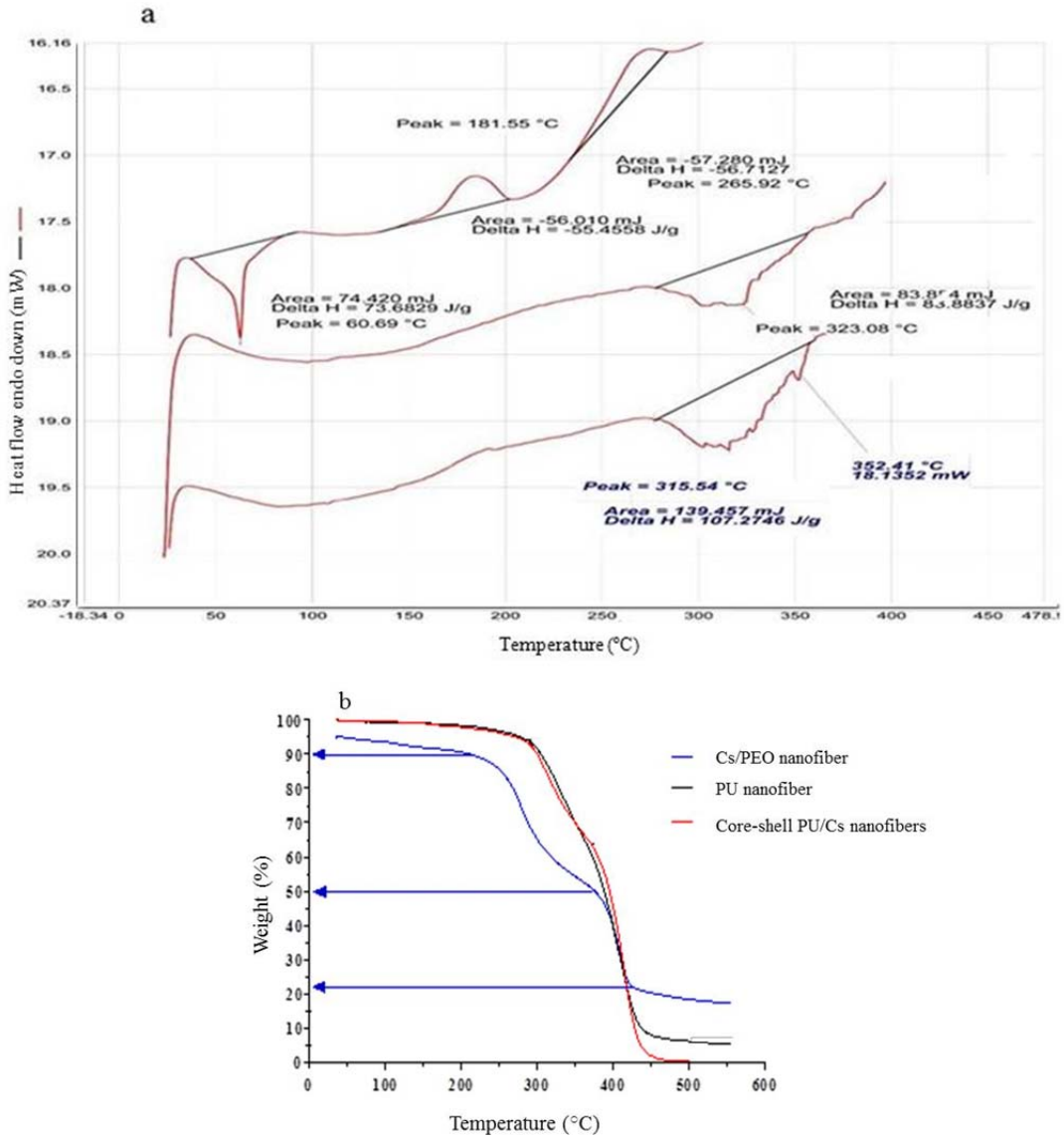

Fig. 5. (a) DSC thermograms and (b) TGA diagrams for Cs/PEO, PU and core-shell PU/Cs nanofibers. DCS, differential scanning calorimetry; TGA, thermogravimetric analysis; Cs, chitosan; PEO, polyethylene oxide; PU, polyurethane.

As it is shown in Fig. 5a (DSC thermograms) each polymer has the distinct thermal behaviors with simultaneous manner leading to broaden the melting temperature (T_m) and glass temperature (T_g) regions in the composition. In TGA analysis shown in Fig. 5b, the resultant Cs-PEO diagrams are presented for mass losses. The first phase of mass losses was at 0-218 °C due to evaporation of the surface water and adsorbed water by Cs (~ 10%). The second phase of mass losses was at 293 °C (between 250-390 °C) due to the thermal degradation of Cs (~ 68%). The second peak of mass losses was at 297-370 °C as result of the thermal degradation of PEO (~ 13%).

DISCUSSION

PU solution (7.5 wt%) was prepared by dissolving PU in THF/DMF blend solvent at different volume ratios including 100:0, 90:10, 80:20, 70:30, 60:40, 50:50, 40:60, 30:70, 20:80, 10:90, and 0:100. The prepared solutions were electrospun by various applied voltage (15, 18, 20 kV) and different needle-collector distance (10, 12, 14 cm). It was found that the optimal parameters were 15 kV, 12 cm, and 0.2 mL/h for the applied voltage, needle-collector distance and flow rate at different THF/DMF blend solvents (Fig. 1a-f), respectively. Fiber diameter of PU nanofiber decreased from 3800 nm to 370 nm as well as mean pore size reduced from 4200 nm to 820 nm by partial substitution of THF with DMF in blend solvent. In nanofibrous scaffolds, cells were filtered and attached on the surface of a scaffold. Higher filtration constant and thus lower SPE is ideal parameter to select a scaffold for cellular attachments (7). The lowest SPE for PU nanofibers was belong to 60:40 and 50:50 THF:DMF ratios, respectively. Therefore, they were selected as optimized solvent composition for PU scaffold. In the next step, PU solutions at 4, 6, 7.5, 8, 9, and 10 wt% were prepared by dissolving PU in THF/DMF at 60:40 % blend solvent at constant voltage of 15 kV, needle-collector distance 12 cm, and corresponding flow rate of 0.2 mL/h. The morphologies of PU nanofibers with variations in concentration at constant ratio of THF/DMF (60:40) solvent are shown in Fig. 2a-c. It was observed that defect free PU nanofibers were obtained at 7.5 wt% concentration. Whereas, nanofiber scaffolds posed the structural imperfections below and above this concentration. Fig. 2d-e showed that core-shell PU/Cs nanofibers were spun with beadless morphology at optimized processing conditions. TEM image confirmed that core-shell nanofibrous structure was formed obviously.

In FTIR spectra, the index peaks belonging to the amine and the hydroxyl groups of chitosan as well as the index peak of N-H group of PU were overlapped and intensified at wavelength 3435 cm^{-1} in the core-shell PU/Cs. This phenomenon confirmed that functional groups of chitosan and PU had the interactions in core-shell structure, because these index peaks were intensified (33). However, the chemical structure of each nanofibers was preserved in the core-shell composition.

In XRD pattern, a decrease in intensity of peak to 19.56 for core-shell PU/Cs nanofibers compared to Cs/PEO nanofiber exhibited that the degree of crystalline phase was lower in the composition compared to shell component. However, it seems the inclusion of Cs/PEO to the shell, did not induce significant variations in crystallinity in the core-shell composition. This phenomenon can be classified as an advantage of coaxial electrospinning for producing a hybrid nanofibers scaffolds which the crystalline phase defined based on the core structure. In DSC thermograms, a sharp peak at 75 °C traced back to the melting process of PEO nanofibers. On the other hand, the index peak at 80 °C is attributed to the dehydration of Cs polymer chains (26,34). As shown in Fig. 5a the thermal behavior of Cs/PEO exhibited an exothermic peak at 60 °C which was lower than the index peaks for PEO and Cs. This reduction could be due to the strong hydrogen bonding between the crystalline chains in PEO and the amorphous chains in Cs in the Cs/PEO blending (26). In addition, the observation of a strong exothermic peak at 110 °C can reflect the dehydration of hydroxyl groups at Cs chains. In general, PU nanofibers have both amorphous and crystalline phase

defined the transmission T_g and the T_m for PU, respectively. By inclusion of Cs/PEO the T_m at composition increased sharply compared to the neat PU nanofibers. This seems that Cs acted as a plasticizer for PU nanofibers leading to an increase in the hydrophilic properties of the composition. In addition, reduced melting point at composition compared to PU nanofibers could be attributed to the increased hydrophilic properties of the composition. As shown in Fig. 5b (TGA analysis), the PU nanofibers degraded at single phase started at 280 °C and terminated at 420 °C while the half degradation was at 380 °C. The core-shell PU/Cs diagrams represented PU nanofiber mass losses, but the degradation occurred in two steps. The first step mass loss was between 280-360 °C related to the PEO degradation while the second step was up to 430 °C attributed to the PU degradation. The thermal degradation of core-shell PU/Cs was similar to PU nanofibers degradation due to the higher PU concentration compared to other components. It can be concluded from DSC and TGA that the thermal behaviors of the core-shell composition is mostly determined based on PU fiber (core) due to its higher content than those of shell components.

CONCLUSION

PU, Cs/PEO, and core-shell PU/Cs nanofibers were electrospun successfully. SEM images revealed that it is possible to produce PU/Cs scaffolds with prefect structure by selecting the solution and processing parameters at optimal conditions.TEM image confirmed that the core-shell nanofibrous structure was formed clearly. FTIR spectra exhibited that functional groups of chitosan and PU had the interactions because their index peaks were intensified in core-shell structure. However, the chemical structure of each nanofibers was preserved in the core-shell composition. DSC thermographs showed that the inclusion of Cs/PEO led to increase sharply in the glass temperature of composition compared to the neat PU nanofibers. It seems that Cs acted as a plasticizer for PU nanofibers leading to an increase in the hydrophilic properties of the composition. The degradation curve of core-shell PU/Cs nanofibers was similar to PU nanofibers, except the mass losses were at two steps. In future, further biological tests should be conducted to evaluate this platform as a nanofibrous scaffold with capabilities to release the bioactive molecules.

ACKNOWLEDGMENTS

This work was financially supported by the Islamic Azad University, South Tehran Branch Tehran, I.R. Iran.

REFERENCES

1. Zhang YZ, Su B, Venugopal J, Ramakrishna S, Lim CT. Biomimetic and bioactive nanofibrous scaffolds from electrospun composite nanofibers. Int J Nanomedicine. 2007;2(4):623-638.
2. Zhang Y, Lim CT, Ramakrishna S, Huang ZM. Recent development of polymer nanofibers for biomedical and biotechnological applications. J Mater Sci Mater Med. 2005;16(10):933-946.
3. He W, Ma Z, Yong T, Teo WE, Ramakrishna S. Fabrication of collagen-coated biodegradable polymer nanofiber mesh and its potential for endothelial cells growth. Biomaterials. 2005;26(36):7606-7615.
4. Das I, De G, Hupa L, Vallittu PK. Porous SiO2 nanofiber grafted novel bioactive glass–ceramic coating: A structural scaffold for uniform apatite precipitation and oriented cell proliferation on inert implant. Mater. Sci Eng C Mater Biol Appl. 2016;62:206-214.
5. Chua KN, Lim WS, Zhang P, Lu H, Wen J, Ramakrishna S, *et al*. Stable immobilization of rat hepatocyte spheroids on galactosylated nanofiber scaffold. Biomaterials. 2005;26(15):2537-2547.
6. Pauly HM, Sathy BN, Olvera D, McCarthy HO, Kelly DJ, Popat KC, *et al*. Hierarchically structured electrospun scaffolds with chemically conjugated growth factor for ligament tissue engineering. Tissue Eng Part A. 2017;23(15-16):823-836.
7. Kazemi Pilehrood M, Dilamian M, Mirian M, Sadeghi-Aliabadi H, Maleknia L, Nousiainen P, *et al*. Nanofibrous chitosan-polyethylene oxide engineered scaffolds: a comparative study between simulated structural characteristics and cells viability. BioMed Res Int. 2014;2014. DOI: 10.1155/2014/438065.
8. Irani M, Mir Mohamad Sadeghi G, Haririan I. Electrospun biocompatible poly (ε-caprolactonediol)-based polyurethane core/shell nanofibrous scaffold for controlled release of temozolomide. Int J Polym Mater. 2017;1-6.
9. Birajdar MS, Lee J. Sonication-triggered zero-order release by uncorking core–shell nanofibers. Chem Eng J. 2016; 288:1-8.

10. Su Y, Su Q, Liu W, Jin G, Mo X, Ramakrishn S. Dual-drug encapsulation and release from core-shell nanofibers. J Biomater Sci Polym Ed. 2012;23(7):861-871.
11. Danielsson C, Ruault S, Simonet M, Neuenschwander P, Frey P. Polyesterurethane foam scaffold for smooth muscle cell tissue engineering. Biomaterials. 2006;27(8):1410-1415.
12. Yannas IV, Lee E, Orgill DP, Skrabut EM, Murphy GF. Synthesis and characterization of a model extracellular matrix that induces partial regeneration of adult mammalian skin. Proc Natl Acad Sci U S A. 1989;86(3):933-937.
13. Griffon DJ, Sedighi MR, Schaeffer DV, Eurell JA, Johnson AL. Chitosan scaffolds: interconnective pore size and cartilage engineering. Acta Biomater. 2006;2(3):313-320.
14. Rahimi M, Mokhtari J. Core-shell hexadecane-polyurethane nanofiber/net structured membrane: Evaluation of surfactant addition on morphology and performance. J Appl Polym Sci. 2017;134(28). DOI: 10.1002/app.45047
15. Chen ZG, Wang PW, Wei B, Mo XM, Cui FZ. Electrospun collagen–chitosan nanofiber: a biomimetic extracellular matrix for endothelial cell and smooth muscle cell. Acta Biomater. 2010;6(2):372-382.
16. Huang C, Chen R, Ke Q, Morsi Y, Zhang K, Mo X. Electrospun collagen-chitosan-TPU nanofibrous scaffolds for tissue engineered tubular grafts. Colloids Surf B Biointerfaces. 2011;82(2):307-315.
17. Chu XH, Shi XL, Feng ZQ, Gu ZZ, Ding YT. Chitosan nanofiber scaffold enhances hepatocyte adhesion and function. Biotechnol Lett. 2009;31(3):347-352.
18. Chen JP, Chen SH, Lai GJ. Preparation and characterization of biomimetic silk fibroin/chitosan composite nanofibers by electrospinning for osteoblasts culture. Nanoscale Res Lett. 2012;7(1):170-180.
19. Mottaghitalab F, Farokhi M, Mottaghitalab V, Ziabari M, Divsalar A, Shokrgozar MA. Enhancement of neural cell lines proliferation using nano-structured chitosan/poly(vinyl alcohol) scaffolds conjugated with nerve growth factor. Carbohydr Polym. 2011;86(2):526-535.
20. Pilehrood MK, Atashi A, Sadeghi-Aliabadi H, Nousiainen P, Harlin A. 3D micro-nano structured hybrid scaffolds: an investigation into the role of nanofiber coating on viability, proliferation and differentiation of seeded mesenchymal stem cells. J Nanosci Nanotechnol. 2016;16(9):9000-9007.
21. Charernsriwilaiwat N, Opanasopit P, Rojanarata T, Ngawhirunpat T. Lysozyme-loaded, electrospun chitosan-based nanofiber mats for wound healing. Int J Pharm. 2012;427(2):379-384.
22. Gu BK, Park SJ, Kim MS, Kang CM, Kim JI, Kim CH. Fabrication of sonicated chitosan nanofiber mat with enlarged porosity for use as hemostatic materials. Carbohydr Polym. 2013;97(1):65-73.
23. Mendes AC, Gorzelanny C, Halter N, Schneider SW, Chronakis IS. Hybrid electrospun chitosan-phospholipids nanofibers for transdermal drug delivery. Int J Pharm. 2016;510(1):48-56.
24. Bazhban M, Nouri M, Mokhtari J. Electrospinning of cyclodextrin functionalized chitosan/PVA nanofibers as a drug delivery system. Chin J Polym Sci. 2013;31(10):1343-1351
25. Cui Z, Zheng Z, Lin L, Si J, Wang Q, Peng X, *et al*. Electrospinning and crosslinking of polyvinyl alcohol/chitosan composite nanofiber for transdermal drug delivery. Adv Polym Technol. 2017. DOI: 10.1002/adv.21850.
26. Dilamian M, Montazer M, Masoumi J. Antimicrobial electrospun membranes of chitosan/poly (ethylene oxide) incorporating poly (hexamethylene biguanide) hydrochloride. Carbohyd Polym. 2013;94:364-371..
27. Kriegel C, Kit KM, McClements DJ, Weiss J. Electrospinning of chitosan-poly (ethylene oxide) blend nanofibers in the presence of micellar surfactant solutions. Polymer. 2009;50(1):189-200.
28. Yeganegi M, Kandel RA, Santerre JP. Characterization of a biodegradable electrospun polyurethane nanofiber scaffold: Mechanical properties and cytotoxicity. Acta Biomater. 2010;6(10):3847-3855.
29. Wright ME, Parrag IC, Yang M, Santerre JP. Electrospun polyurethane nanofiber scaffolds with ciprofloxacin oligomer versus free ciprofloxacin: Effect on drug release and cell attachment. J Control Release. 2017;250:107-115.
30. Akduman C, Özgüney I, Kumbasar EPA. Preparation and characterization of naproxen-loaded electrospun thermoplastic polyurethane nanofibers as a drug delivery system. Mater Sci Eng C Mater Biol Appl. 2016;64:383-390.
31. Gencturk A, Kahraman E, Güngör S, Özhan G, Özsoy Y, Sarac AS. Polyurethane/hydroxypropyl cellulose electrospun nanofiber mats as potential transdermal drug delivery system: characterization studies and *in vitro* assays. Artifi Cells Nanomed Biotechnol. 2017;45(3):655-664.
32. Kazemi Pilehrood M, Heikkilä P, Harlin A. Simulation of structural characteristics and depth filtration elements in interconnected nanofibrous membrane based on adaptive image analysis. World J Nano Sci. Eng. 2013;3(1):6-16.
33. Lee SJ, Heo DN, Moon JH, Park HN, Ko WK, Bae MS, *et al*. Chitosan/polyurethane blended fiber sheets containing silver sulfadiazine for use as an antimicrobial wound dressing. J Nanosci Nanotechnol. 2014;14(10):7488-7494.
34. Neto CGT, Giacometti JA, Job AE, Ferreira FC, Fonseca JLC, Pereira MR. Thermal analysis of chitosan based networks. Carbohyd Polym. 2005;62(2):97-103.